Supplementary Information

# Tellurium Recovery from the Thermoelectric Materials Bismuth Telluride and Antimony Telluride by Chemical Vapour Transport

Julian Burkhart,[a] Lucas H. Bemfert,[a] Eliane L. Mitura,[a] Moritz Maxeiner,[a] Ruben Maile,[a] Alexander E. Sedykh[a] and Klaus Müller-Buschbaum*[ab]

[a.] Institute of Inorganic and Analytical Chemistry, Justus-Liebig-University Giessen, Heinrich-Buff-Ring 17, 35392 Giessen, Germany.
E-Mail: kmbac@uni-giessen.de
Web: https://www.uni-giessen.de/de/fbz/fb08/Inst/iaac/mueller-buschbaum

[b.] Center for Materials Research (LAMA), Justus-Liebig-University Giessen, Heinrich-Buff-Ring 16, 35392 Giessen, Germany.

## Contents

# Chemical vapour transport (CVT) in closed experimental setups

Table S1: Parameters and results of the closed $Bi_2Te_3/S$ temperature gradient investigations.

| System | $T_1$ / °C | $T_2$ / °C | Te:S molar ratio | t / h | Transport rate (Te) / mg · h$^{-1}$ | Recovery rate (Te) / % · h$^{-1}$ | Recovery yield / % |
|---|---|---|---|---|---|---|---|
| $Bi_2Te_3/S$ | 325 | 425 | 1:2 | 72 | 4.0 | 1.3 | 96.6 |
| $Bi_2Te_3/S$ | 325 | 425 | 1:2 | 72 | 4.0 | 1.4 | 97.5 |
| $Bi_2Te_3/S$ | 325 | 425 | 1:2 | 72 | 4.1 | 1.4 | 99.8 |
| $Bi_2Te_3/S$ | 350 | 425 | 1:2 | 72 | 3.9 | 1.3 | 94.1 |
| $Bi_2Te_3/S$ | 350 | 425 | 1:2 | 72 | 3.6 | 1.2 | 86.9 |
| $Bi_2Te_3/S$ | 350 | 425 | 1:2 | 72 | 4.1 | 1.4 | 98.7 |
| $Bi_2Te_3/S$ | 300 | 400 | 1:2 | 72 | 3.9 | 1.3 | 95.0 |
| $Bi_2Te_3/S$ | 300 | 400 | 1:2 | 72 | 4.0 | 1.3 | 95.6 |
| $Bi_2Te_3/S$ | 300 | 400 | 1:2 | 72 | 3.6 | 1.2 | 86.3 |
| $Bi_2Te_3/S$ | 325 | 400 | 1:2 | 72 | 4.1 | 1.4 | 99.0 |
| $Bi_2Te_3/S$ | 325 | 400 | 1:2 | 72 | 3.9 | 1.3 | 94.4 |
| $Bi_2Te_3/S$ | 325 | 400 | 1:2 | 72 | 3.4 | 1.1 | 81.6 |
| $Bi_2Te_3/S$ | 350 | 400 | 1:2 | 72 | 2.2 | 0.7 | 53.3 |
| $Bi_2Te_3/S$ | 350 | 400 | 1:2 | 72 | 3.0 | 1.0 | 72.6 |
| $Bi_2Te_3/S$ | 350 | 400 | 1:2 | 72 | 3.5 | 1.2 | 83.4 |
| $Bi_2Te_3/S$ | 300 | 375 | 1:2 | 72 | 3.5 | 1.2 | 84.5 |
| $Bi_2Te_3/S$ | 300 | 375 | 1:2 | 72 | 2.2 | 0.7 | 51.9 |
| $Bi_2Te_3/S$ | 300 | 375 | 1:2 | 72 | 2.4 | 0.8 | 56.6 |
| $Bi_2Te_3/S$ | 325 | 375 | 1:2 | 72 | 2.0 | 0.7 | 48.0 |
| $Bi_2Te_3/S$ | 325 | 375 | 1:2 | 72 | 2.9 | 1.0 | 68.7 |
| $Bi_2Te_3/S$ | 325 | 375 | 1:2 | 72 | 2.3 | 0.8 | 54.9 |
| $Bi_2Te_3/S$ | 350 | 375 | 1:2 | 72 | 1.1 | 0.4 | 26.4 |
| $Bi_2Te_3/S$ | 350 | 375 | 1:2 | 72 | 1.7 | 0.6 | 39.8 |
| $Bi_2Te_3/S$ | 350 | 375 | 1:2 | 72 | 1.7 | 0.6 | 40.5 |

Table S2: Parameters and results of the closed $Sb_2Te_3/S$ temperature gradient investigations.

| System | $T_1$ / °C | $T_2$ / °C | Te:S molar ratio | t / h | Transport rate (Te) / mg · h$^{-1}$ | Recovery rate (Te) / % · h$^{-1}$ | Recovery yield / % |
|---|---|---|---|---|---|---|---|
| $Sb_2Te_3/S$ | 325 | 425 | 1:2 | 72 | 4.1 | 1.4 | 97.7 |
| $Sb_2Te_3/S$ | 325 | 425 | 1:2 | 72 | 3.8 | 1.3 | 91.2 |
| $Sb_2Te_3/S$ | 325 | 425 | 1:2 | 72 | 4.0 | 1.3 | 96.2 |
| $Sb_2Te_3/S$ | 350 | 425 | 1:2 | 72 | 2.5 | 0.8 | 60.5 |
| $Sb_2Te_3/S$ | 350 | 425 | 1:2 | 72 | 3.1 | 1.0 | 75.0 |
| $Sb_2Te_3/S$ | 350 | 425 | 1:2 | 72 | 3.0 | 1.0 | 73.1 |
| $Sb_2Te_3/S$ | 300 | 400 | 1:2 | 72 | 3.1 | 1.0 | 74.9 |
| $Sb_2Te_3/S$ | 300 | 400 | 1:2 | 72 | 3.5 | 1.2 | 85.0 |
| $Sb_2Te_3/S$ | 300 | 400 | 1:2 | 72 | 3.9 | 1.3 | 94.6 |
| $Sb_2Te_3/S$ | 325 | 400 | 1:2 | 72 | 2.6 | 0.9 | 62.8 |
| $Sb_2Te_3/S$ | 325 | 400 | 1:2 | 72 | 3.4 | 1.1 | 81.5 |
| $Sb_2Te_3/S$ | 325 | 400 | 1:2 | 72 | 3.5 | 1.2 | 83.8 |
| $Sb_2Te_3/S$ | 350 | 400 | 1:2 | 72 | 1.6 | 0.5 | 38.9 |
| $Sb_2Te_3/S$ | 350 | 400 | 1:2 | 72 | 2.1 | 0.7 | 51.3 |
| $Sb_2Te_3/S$ | 350 | 400 | 1:2 | 72 | 2.2 | 0.7 | 53.0 |
| $Sb_2Te_3/S$ | 300 | 375 | 1:2 | 72 | 2.5 | 0.8 | 59.6 |
| $Sb_2Te_3/S$ | 300 | 375 | 1:2 | 72 | 2.4 | 0.8 | 57.8 |
| $Sb_2Te_3/S$ | 300 | 375 | 1:2 | 72 | 2.5 | 0.8 | 60.5 |
| $Sb_2Te_3/S$ | 325 | 375 | 1:2 | 72 | 1.9 | 0.6 | 44.9 |
| $Sb_2Te_3/S$ | 325 | 375 | 1:2 | 72 | 2.3 | 0.8 | 54.5 |
| $Sb_2Te_3/S$ | 325 | 375 | 1:2 | 72 | 1.9 | 0.7 | 47.0 |
| $Sb_2Te_3/S$ | 350 | 375 | 1:2 | 72 | 0.9 | 0.3 | 21.8 |
| $Sb_2Te_3/S$ | 350 | 375 | 1:2 | 72 | 1.1 | 0.4 | 26.6 |
| $Sb_2Te_3/S$ | 350 | 375 | 1:2 | 72 | 1.2 | 0.4 | 28.1 |

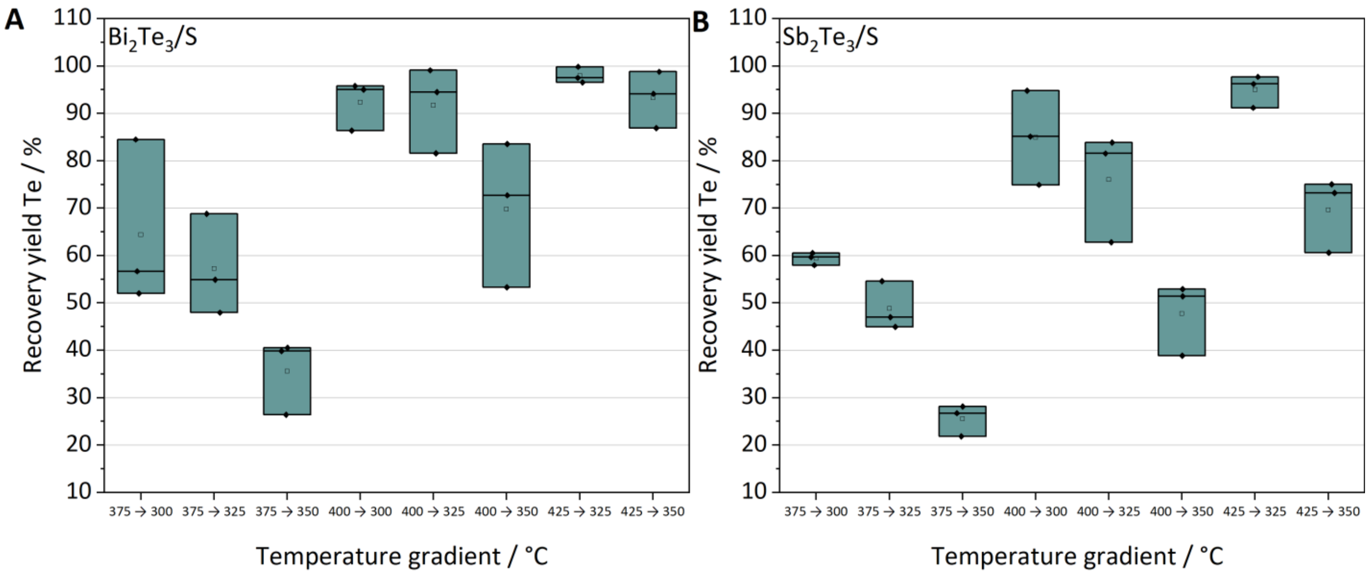


Figure S1: Box diagrams of recovery yields in closed experimental setups for both telluride systems (A: $Bi_2Te_3/S$, B: $Sb_2Te_3/S$). Eight different temperature gradients in the range of 300-425 °C were used. Furthermore, each black point represents one ampoule. This data was used to create the heat maps in Figure 3.

Table S3: Parameters and results of the closed $Bi_2Te_3/S$ Te:S molar ratio and reaction time investigations.

| System | $T_1$ / °C | $T_2$ / °C | Te:S molar ratio | t / h | Transport rate (Te) / mg · h$^{-1}$ | Recovery rate (Te) / % · h$^{-1}$ | Recovery yield / % |
|---|---|---|---|---|---|---|---|
| $Bi_2Te_3/S$ | 325 | 425 | 1:2 | 72 | 4.0 | 1.4 | 97.5 |
| $Bi_2Te_3/S$ | 325 | 425 | 1:2 | 72 | 4.1 | 1.4 | 99.8 |
| $Bi_2Te_3/S$ | 325 | 425 | 1:1.25 | 72 | 4.1 | 1.4 | 98.4 |
| $Bi_2Te_3/S$ | 325 | 425 | 1:1.25 | 72 | 4.1 | 1.4 | 97.8 |
| $Bi_2Te_3/S$ | 325 | 425 | 1:2 | 48 | 5.4 | 1.8 | 86.7 |
| $Bi_2Te_3/S$ | 325 | 425 | 1:2 | 48 | 6.1 | 2.0 | 98.1 |
| $Bi_2Te_3/S$ | 325 | 425 | 1:1.25 | 48 | 5.3 | 1.8 | 84.4 |
| $Bi_2Te_3/S$ | 325 | 425 | 1:1.25 | 48 | 5.7 | 1.9 | 91.4 |
| $Bi_2Te_3/S$ | 325 | 425 | 1:2 | 24 | 6.0 | 2.0 | 47.8 |
| $Bi_2Te_3/S$ | 325 | 425 | 1:2 | 24 | 7.1 | 2.4 | 57.1 |
| $Bi_2Te_3/S$ | 325 | 425 | 1:1.25 | 24 | 6.8 | 2.3 | 54.4 |
| $Bi_2Te_3/S$ | 325 | 425 | 1:1.25 | 24 | 6.2 | 2.1 | 50.1 |
| $Bi_2Te_3/S$ | 325 | 375 | 1:2 | 72 | 1.9 | 0.6 | 45.4 |
| $Bi_2Te_3/S$ | 325 | 375 | 1:2 | 72 | 2.7 | 0.9 | 65.6 |
| $Bi_2Te_3/S$ | 325 | 375 | 1:1.25 | 72 | 2.1 | 0.7 | 50.7 |
| $Bi_2Te_3/S$ | 325 | 375 | 1:1.25 | 72 | 2.9 | 1.0 | 69.6 |
| $Bi_2Te_3/S$ | 325 | 375 | 1:2 | 48 | 2.6 | 0.9 | 41.8 |
| $Bi_2Te_3/S$ | 325 | 375 | 1:2 | 48 | 2.8 | 0.9 | 44.7 |
| $Bi_2Te_3/S$ | 325 | 375 | 1:1.25 | 48 | 2.7 | 0.9 | 43.6 |
| $Bi_2Te_3/S$ | 325 | 375 | 1:1.25 | 48 | 2.7 | 0.9 | 43.6 |
| $Bi_2Te_3/S$ | 325 | 375 | 1:2 | 24 | 2.9 | 1.0 | 23.1 |
| $Bi_2Te_3/S$ | 325 | 375 | 1:2 | 24 | 2.8 | 0.9 | 22.2 |
| $Bi_2Te_3/S$ | 325 | 375 | 1:1.25 | 24 | 2.2 | 0.7 | 17.4 |
| $Bi_2Te_3/S$ | 325 | 375 | 1:1.25 | 24 | 2.6 | 0.9 | 20.9 |

Table S4: Parameters and results of the closed $Bi_2Te_3$/S recovery rate investigations.

| System | $T_1$ / °C | $T_2$ / °C | Te:S molar ratio | t / h | Transport rate (Te) / mg · h$^{-1}$ | Recovery rate (Te) / % · h$^{-1}$ | Recovery yield / % |
|---|---|---|---|---|---|---|---|
| $Bi_2Te_3$/S | 325 | 425 | 1:1.25 | 1 | 4.1 | 1.4 | 1.4 |
| $Bi_2Te_3$/S | 325 | 425 | 1:1.25 | 1 | 6.5 | 2.2 | 2.2 |
| $Bi_2Te_3$/S | 325 | 425 | 1:1.25 | 2 | 5.6 | 1.9 | 3.8 |
| $Bi_2Te_3$/S | 325 | 425 | 1:1.25 | 2 | 5.4 | 1.8 | 3.6 |
| $Bi_2Te_3$/S | 325 | 425 | 1:1.25 | 4 | 7.2 | 2.4 | 9.6 |
| $Bi_2Te_3$/S | 325 | 425 | 1:1.25 | 4 | 5.4 | 1.8 | 7.3 |
| $Bi_2Te_3$/S | 325 | 425 | 1:1.25 | 8 | 5.4 | 1.8 | 14.4 |
| $Bi_2Te_3$/S | 325 | 425 | 1:1.25 | 8 | 6.9 | 2.3 | 18.4 |
| $Bi_2Te_3$/S | 325 | 425 | 1:1.25 | 24 | 6.2 | 2.1 | 50.1 |
| $Bi_2Te_3$/S | 325 | 425 | 1:1.25 | 24 | 6.8 | 2.3 | 54.4 |
| $Bi_2Te_3$/S | 325 | 425 | 1:1.25 | 48 | 5.3 | 1.8 | 84.4 |
| $Bi_2Te_3$/S | 325 | 425 | 1:1.25 | 48 | 5.7 | 1.9 | 91.4 |
| $Bi_2Te_3$/S | 325 | 375 | 1:1.25 | 72 | 4.1 | 1.4 | 98.4 |
| $Bi_2Te_3$/S | 325 | 375 | 1:1.25 | 72 | 4.1 | 1.4 | 97.8 |

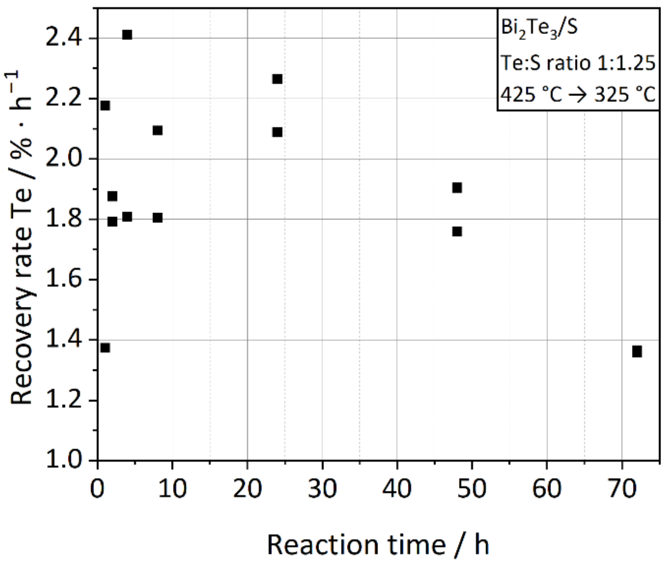


Figure S2: Recovery rates in closed experimental setups in dependence on different reaction times (1 h, 2 h, 4 h, 8 h, 24 h, 48 h, 72 h) for the system $Bi_2Te_3$/S with a Te:S ratio of 1:1.25 at a temperature gradient of 425 °C → 325 °C.

## Differential scanning calorimetry (DSC)

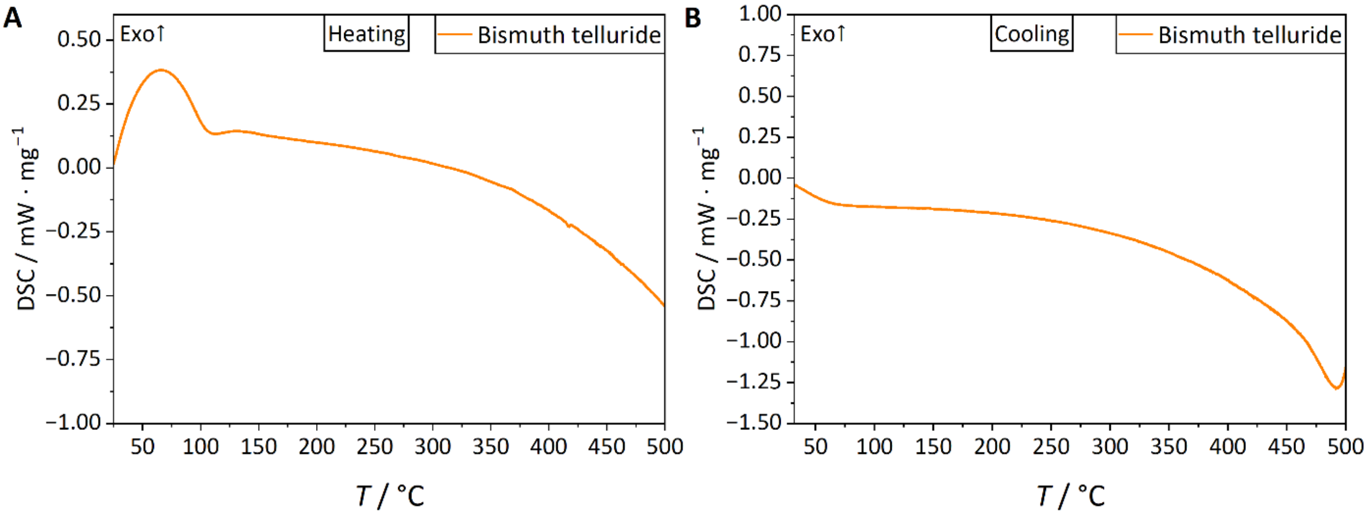


Figure S3: Heat flow determined by DSC (A: Heating and B: Cooling) of a bismuth telluride reference sample.

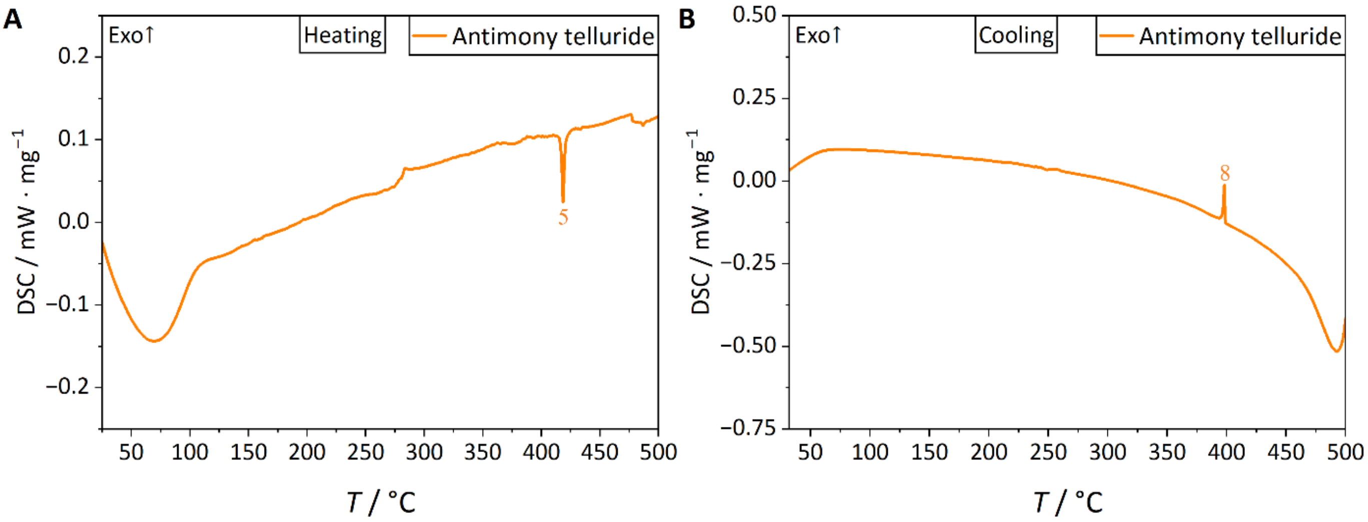


Figure S4: Heat flow determined by DSC (A: Heating and B: Cooling) of an antimony telluride reference sample. Additionally, eutectic temperature of antimony and tellurium (5) and crystallisation (8) of this melt is marked as in Figure 3 in the main article.

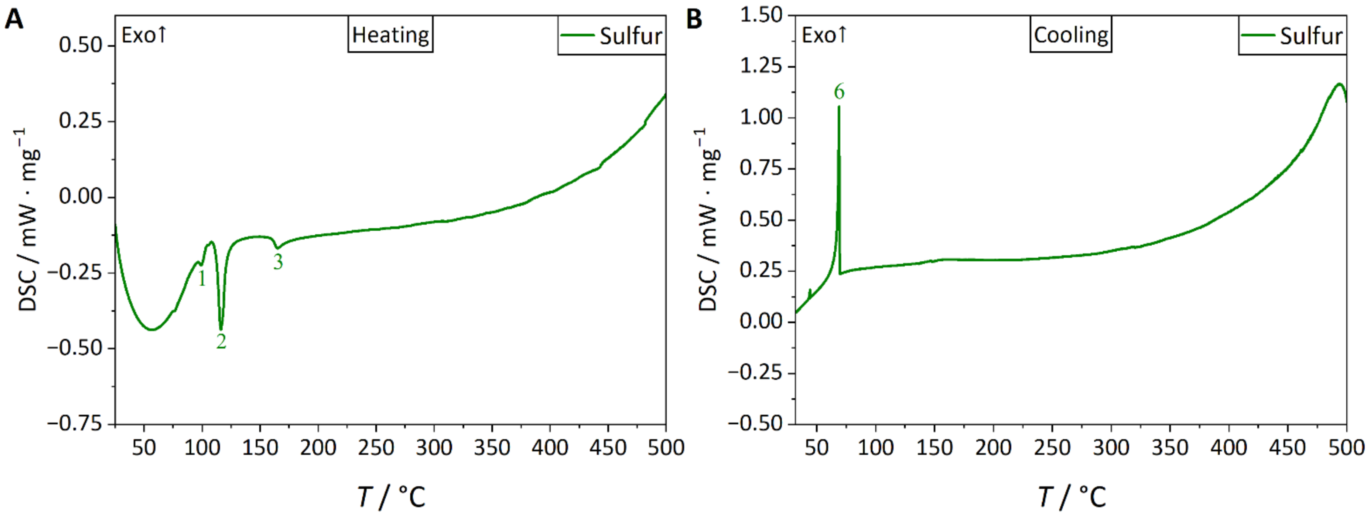


Figure S5:Heat flow determined by DSC (A: Heating and B: Cooling) of a sulfur reference sample. Additionally, transition of orthorhombic α-sulfur to monoclinic β-sulfur (1), melting (2), polymerization (3) and crystallisation (6) of sulfur is marked as in Figure 3 in the main article.

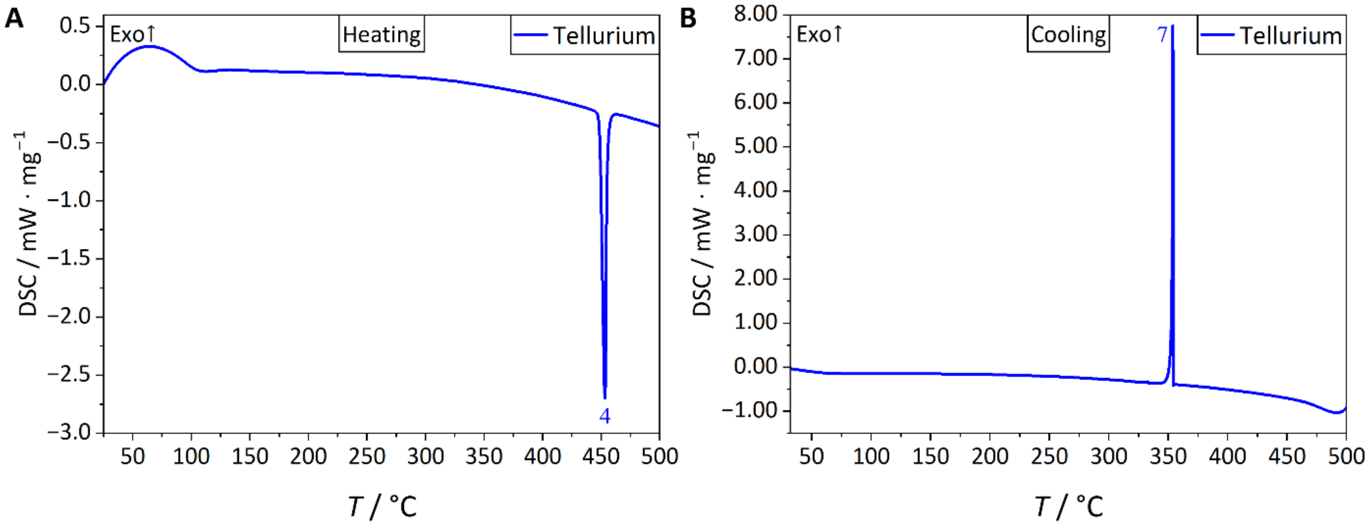


Figure S6: Heat flow determined by DSC (A: Heating and B: Cooling) of a tellurium reference sample. Additionally, melting (4) and crystallisation (7) of tellurium is marked as in Figure 3 in the main article.

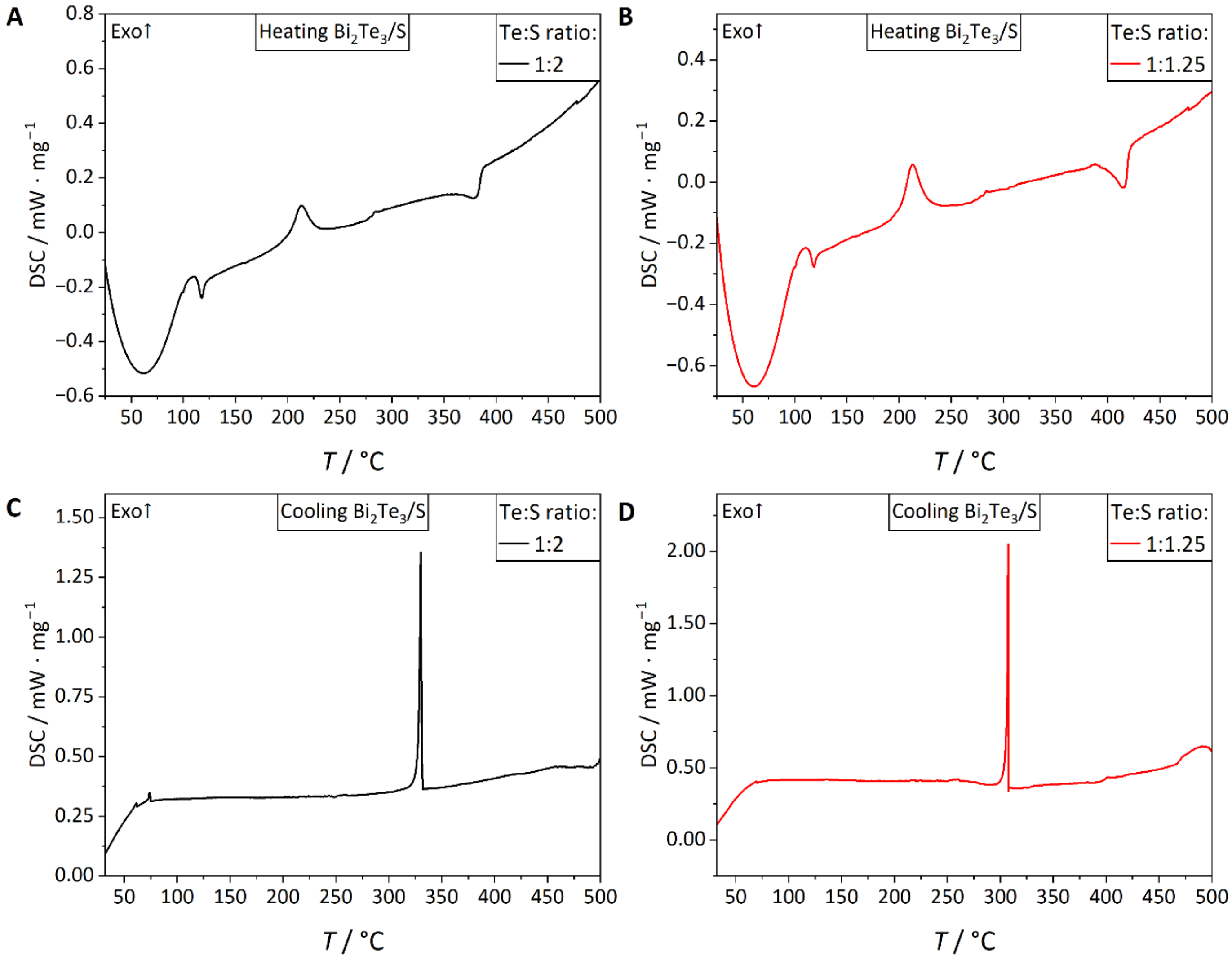


Figure S7: Heat flow determined by DSC (A&B: Heating, C&D: Cooling) of bismuth telluride and sulfur mixtures with two different Te:S molar ratios (Black: 1:2, Red: 1:1.25).

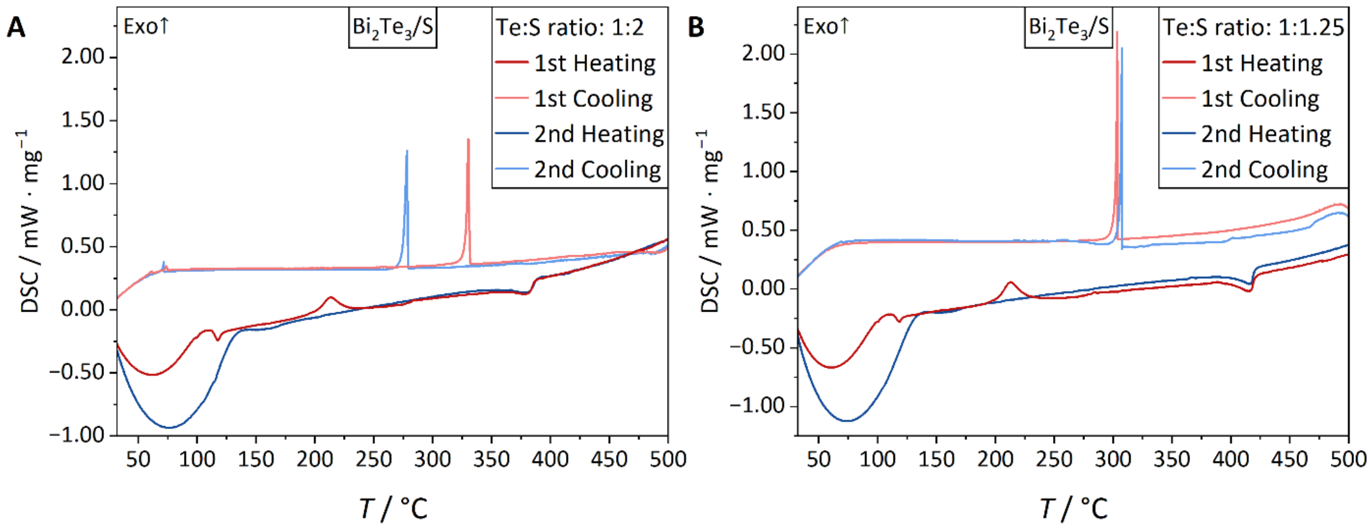


Figure S8: Two DSC-cycles (red: First cycle, blue: Second cycle) of bismuth telluride and sulfur mixtures with two different Te:S molar ratios (A:1:2, B: 1:1.25).

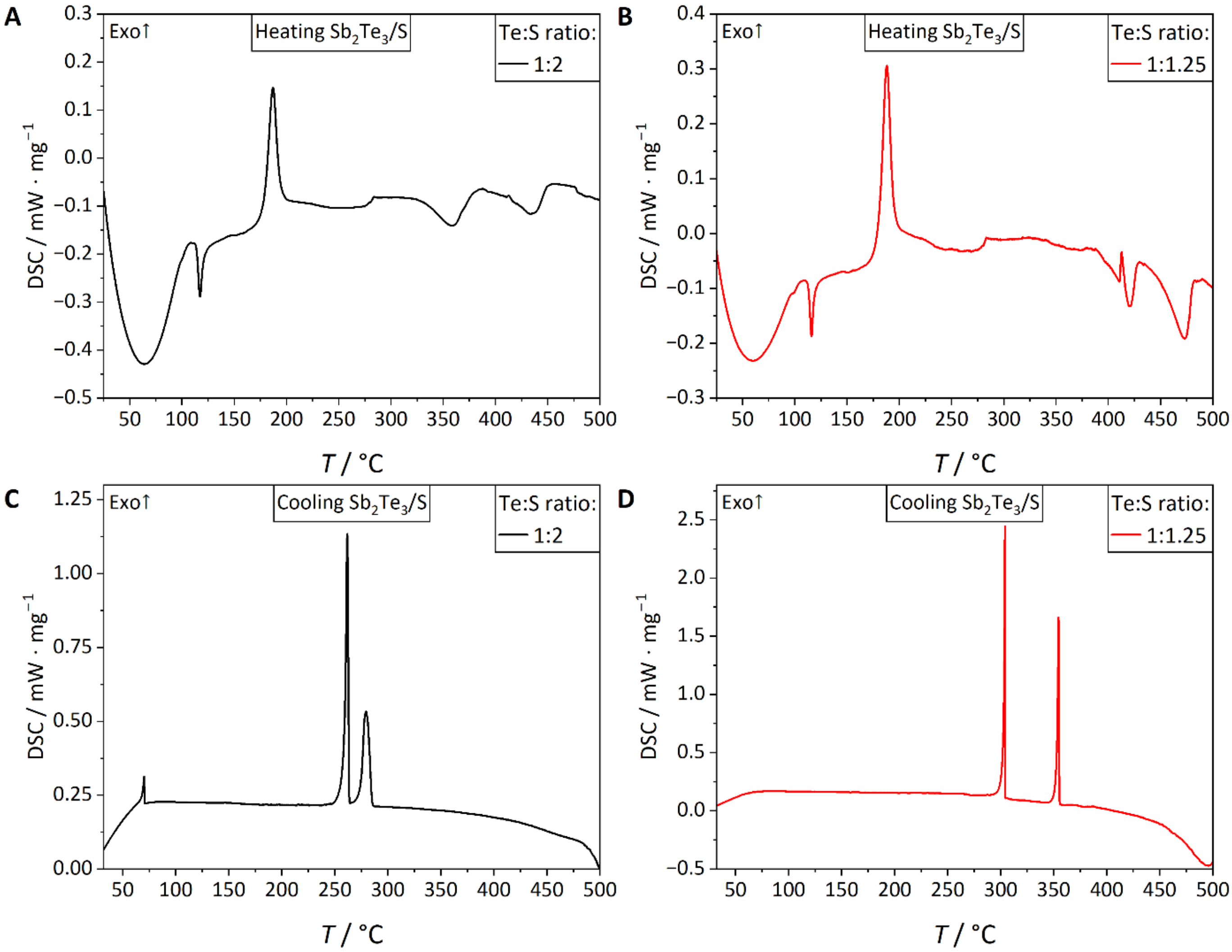


Figure S9: Heat flow determined by DSC (A&B: Heating, C&D: Cooling) of antimony telluride and sulfur mixtures with two different Te:S molar ratios (Black: 1:2, Red: 1:1.25).

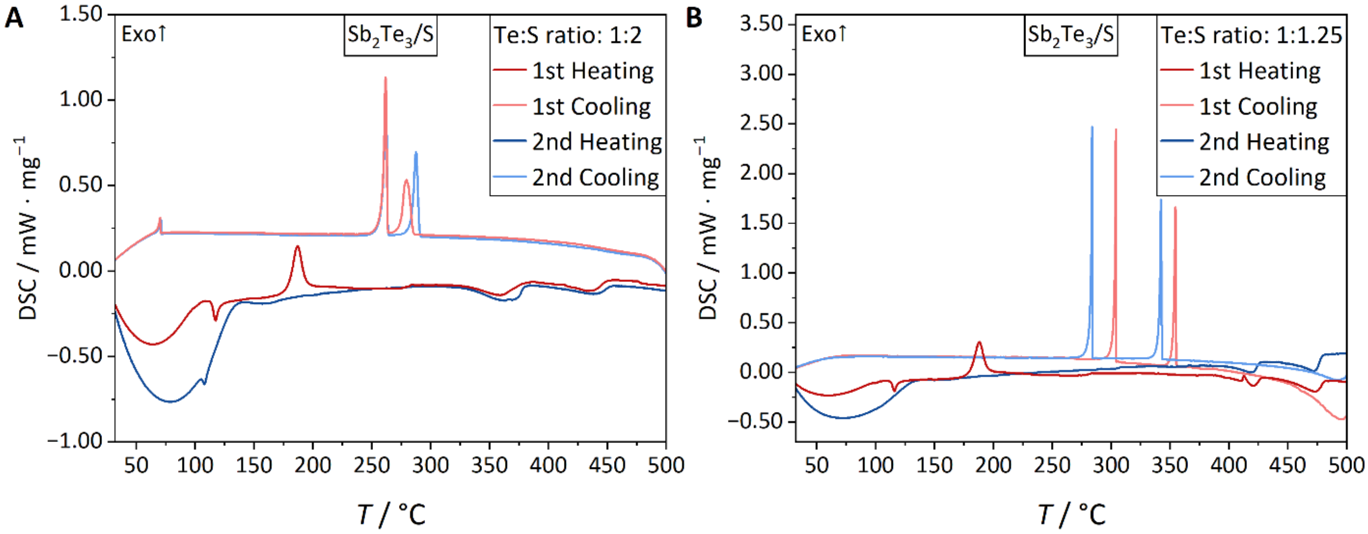


Figure S10: Two DSC-cycles (red: First cycle, blue: Second cycle) of antimony telluride and sulfur mixtures with two different Te:S molar ratios (A:1:2, B: 1:1.25).

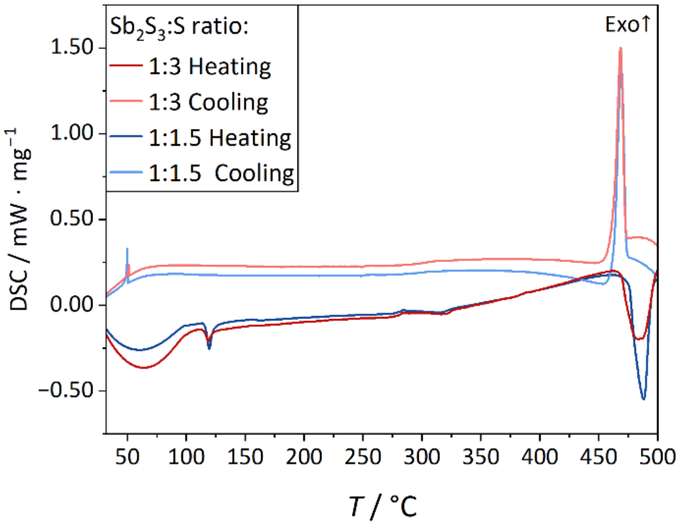


Figure S11: DSC-cycles of antimony sulfide and sulfur mixtures with two different $Sb_2S_3$:S molar ratios (red: 1:1, blue: 1:0.25).

## Powder X-ray diffractometry (PXRD)

In all shown PXRDs of the source, lower tellurium recovery rates are the reason why tellurium reflections are still observable.

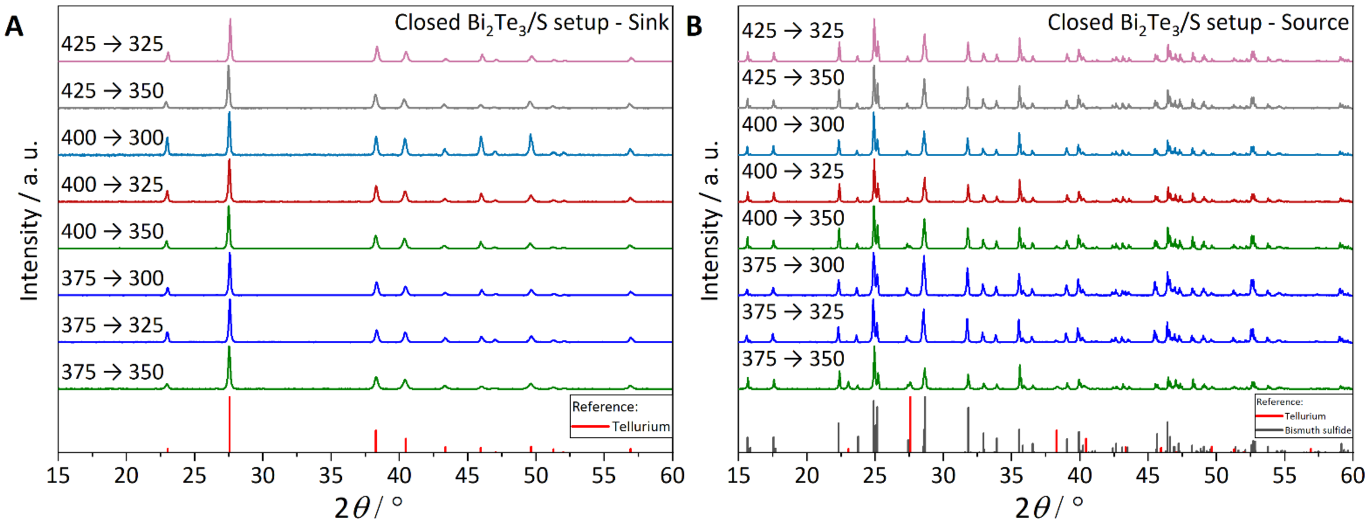


Figure S12: One exemplary PXRD-data for each closed experimental $Bi_2Te_3$/S setup (A: Sink and B: Source) with varying temperature gradient. Additionally, reference patterns are shown for tellurium[1] and bismuth sulfide[2].

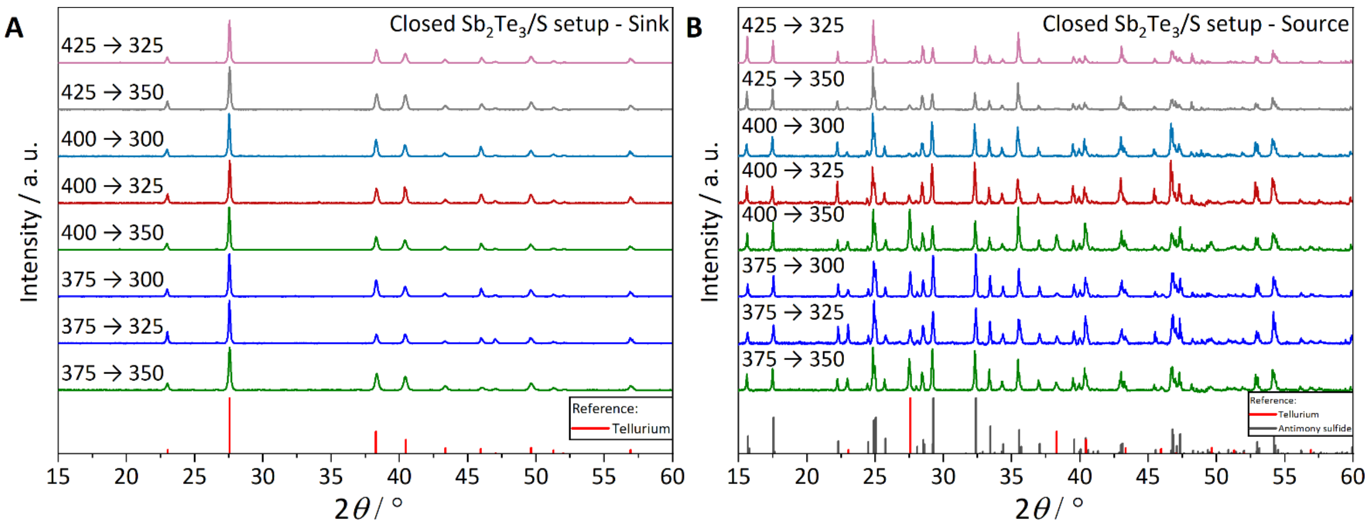


Figure S13: One exemplary PXRD-data for each closed experimental $Sb_2Te_3$/S setup (A: Sink and B: Source) with varying temperature gradient. Additionally, reference patterns are shown for tellurium[1] and antimony sulfide[3].

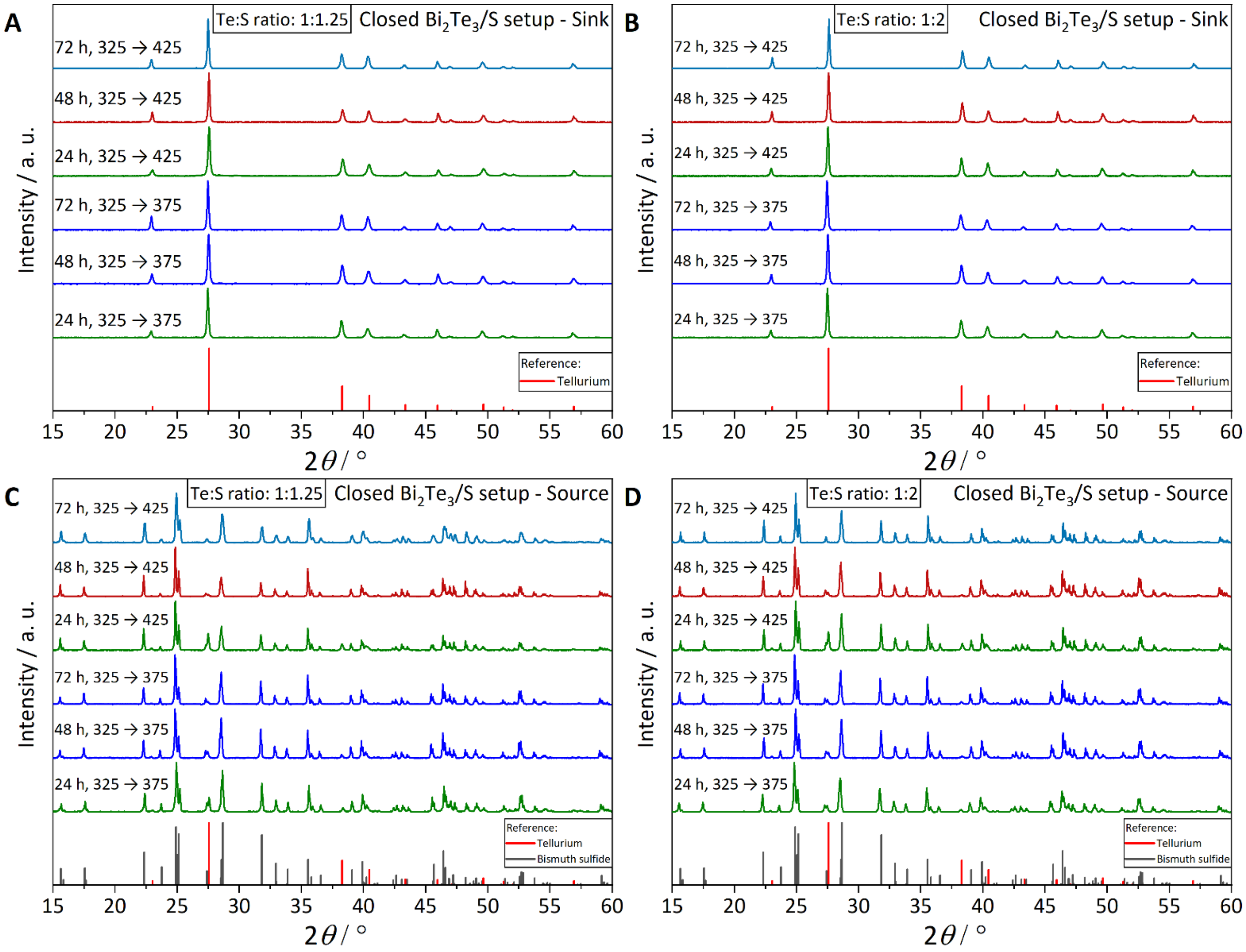


Figure S14: One exemplary PXRD-data for each closed experimental $Bi_2Te_3$/S setup (A, B: Sink and C, D: Source) with varying Te:S molar ratio (A, C: 1:1.25 or B, D: 1:2) at different temperature gradients (325 → 425 or 325 → 375) and reaction times (24 h, 48 h, 72 h). Additionally, reference patterns are shown for tellurium[1] and bismuth sulfide[2].

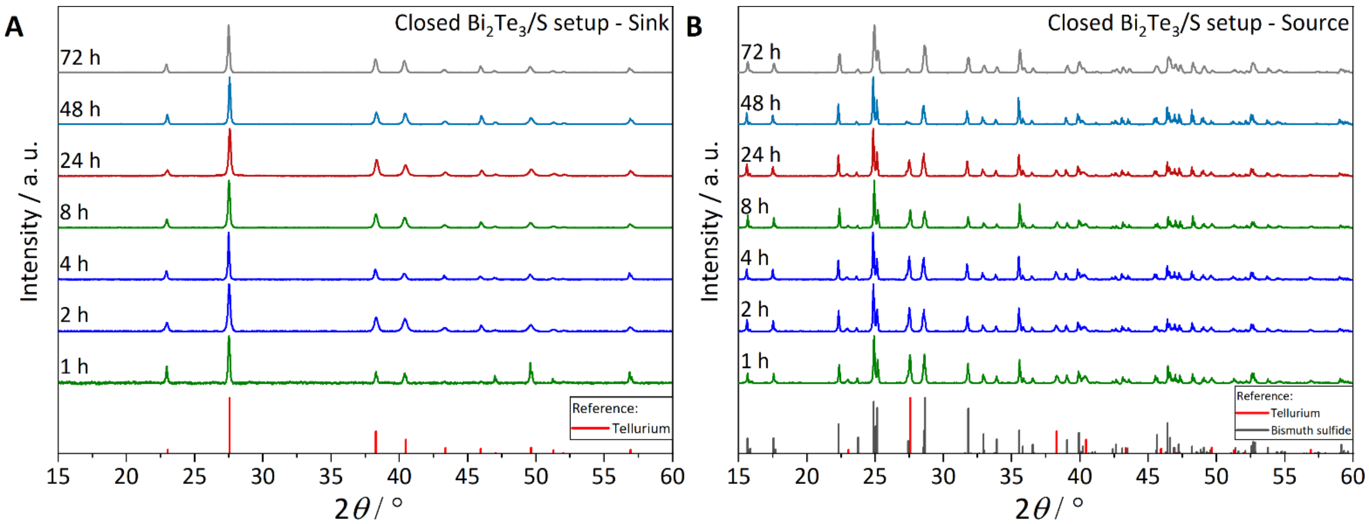


Figure S15: One exemplary PXRD-data for each closed experimental $Bi_2Te_3$/S setup (A: Sink and B: Source) with varying reaction time (1 h, 2 h, 4 h, 8 h, 24 h, 48 h, 72 h). Additionally, reference patterns are shown for tellurium[1] and bismuth sulfide[2].

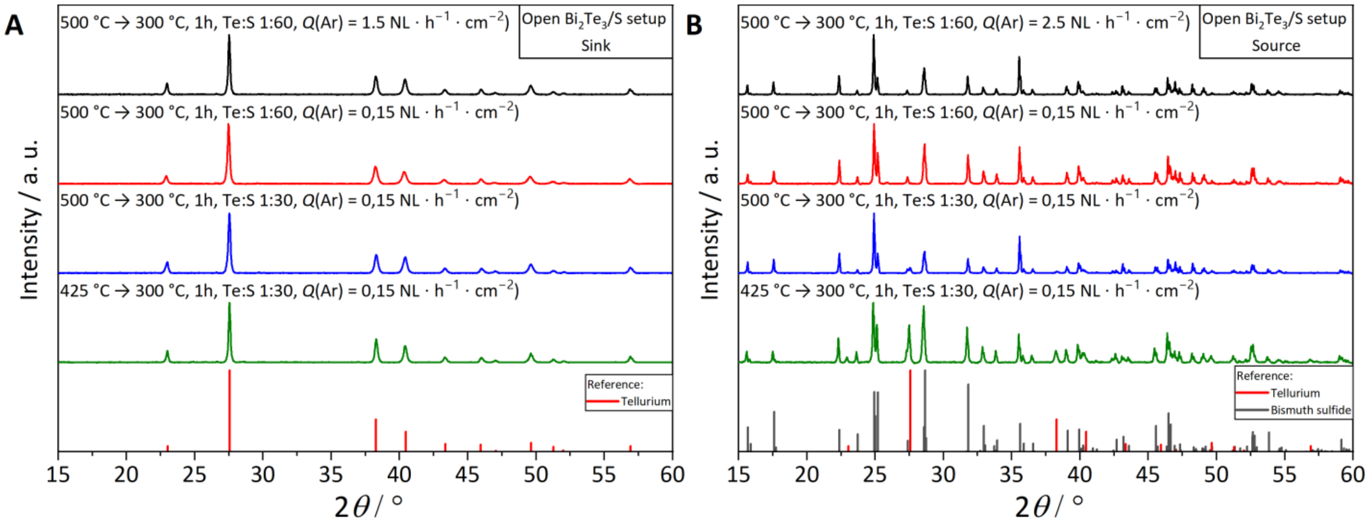


Figure S16: PXRD-data of four different open experimental setups (A: Sink and B: Source) for the $Bi_2Te_3$/S system. Additionally, reference patterns are shown for tellurium[1] and bismuth sulfide[2].

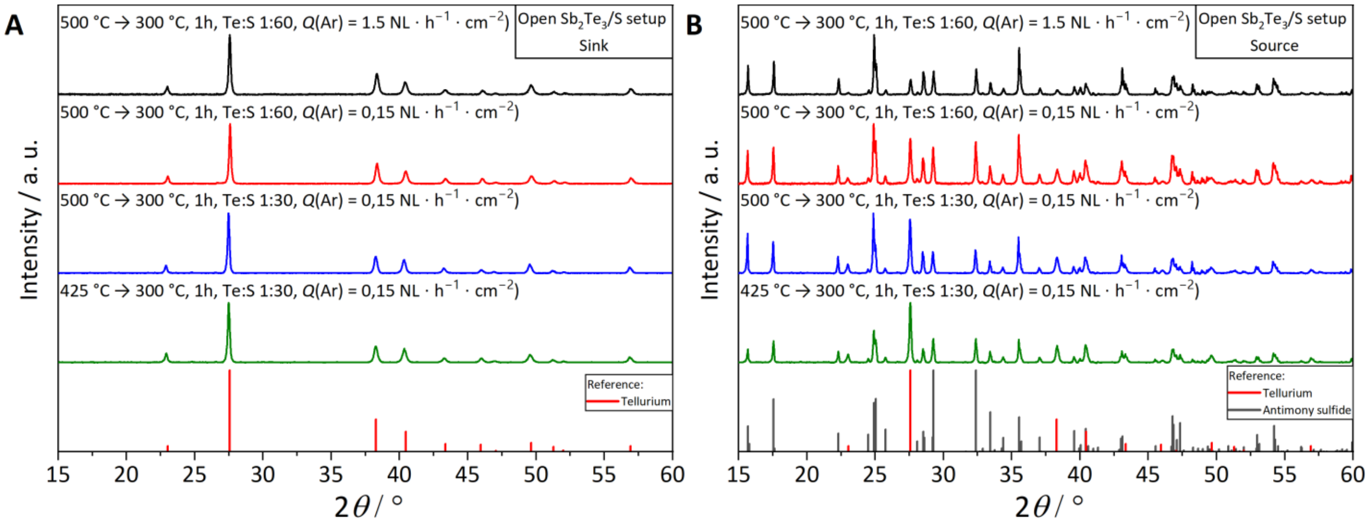


Figure S17: PXRD-data of four different open experimental setups (A: Sink and B: Source) for the $Sb_2Te_3$/S system. Additionally, reference patterns are shown for tellurium[1] and antimony sulfide[3].

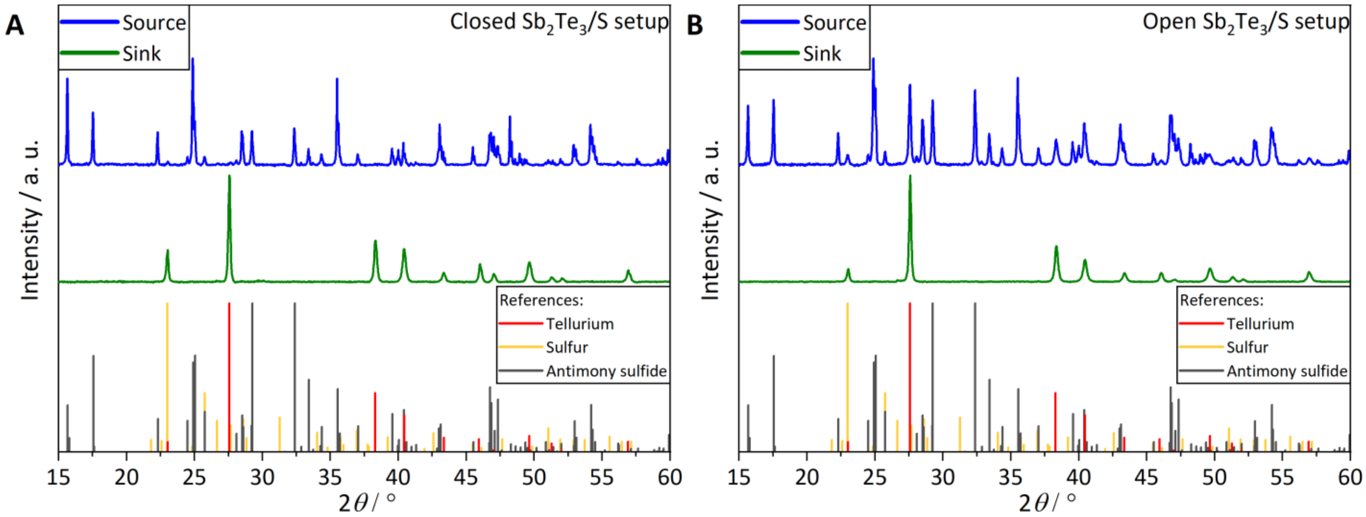


Figure S18: PXRD-data of source (blue diffractogram) and sink (green diffractogram) products of (A) best closed and (B) best open experimental $Sb_2Te_3$/S setup. Additionally, references for tellurium[1], sulfur[4] and antimony sulfide[3] are shown.

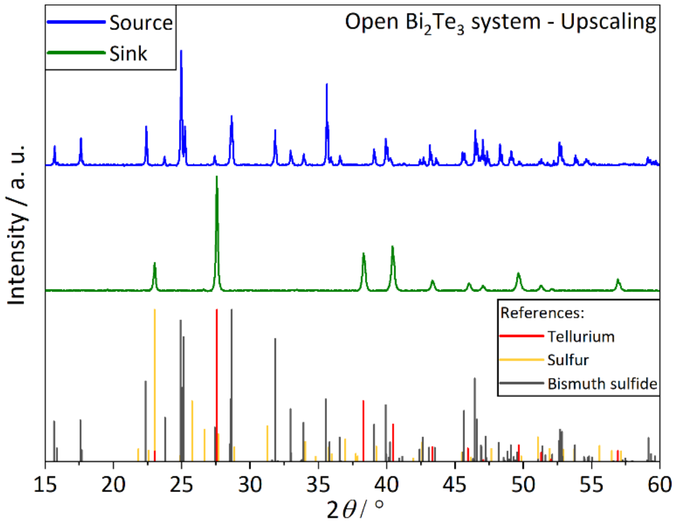


Figure S19: PXRD-data of source (blue diffractogram) and sink (green diffractogram) products of upscaling of open experimental $Bi_2Te_3$/S setup. Additionally, references for tellurium[1], sulfur[4] and bismuth sulfide[2] are shown.

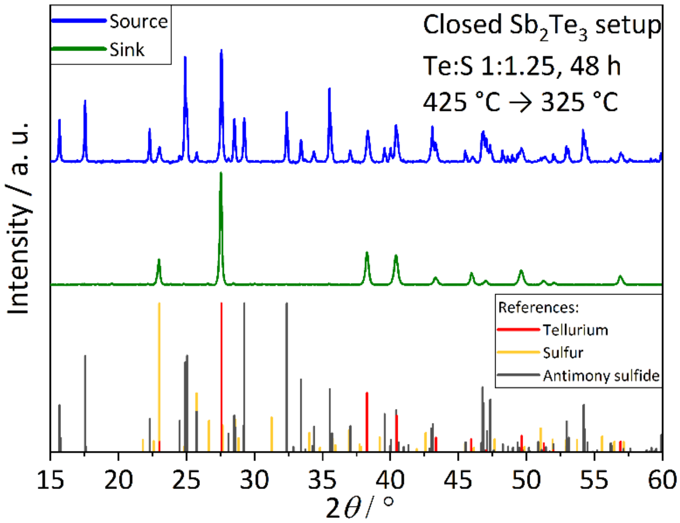


Figure S20: PXRD-data of source (blue diffractogram) and sink (green diffractogram) products of the $Sb_2Te_3$/S experimental setup with a reaction of 48 h and a Te:S molar ratio of 1:1.25 at a temperature gradient of 425 °C → 325 °C. Additionally, references for tellurium[1], sulfur[4] and antimony sulfide[3] are shown.

## Raman spectroscopy

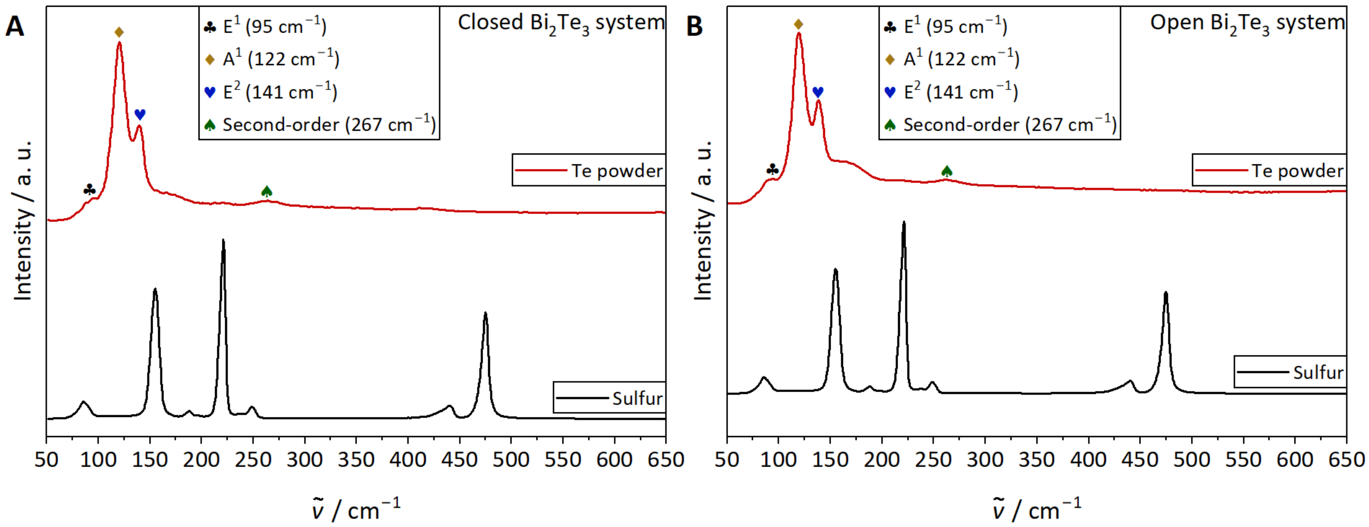


Figure S21: Raman spectra for tellurium recovered in (A) best closed and (B) best open experimental $Bi_2Te_3$/S setup. A reference measurement of sulfur is also shown, and the specific Raman modes of tellurium are marked.

# Energy dispersive X-ray analysis (EDX)

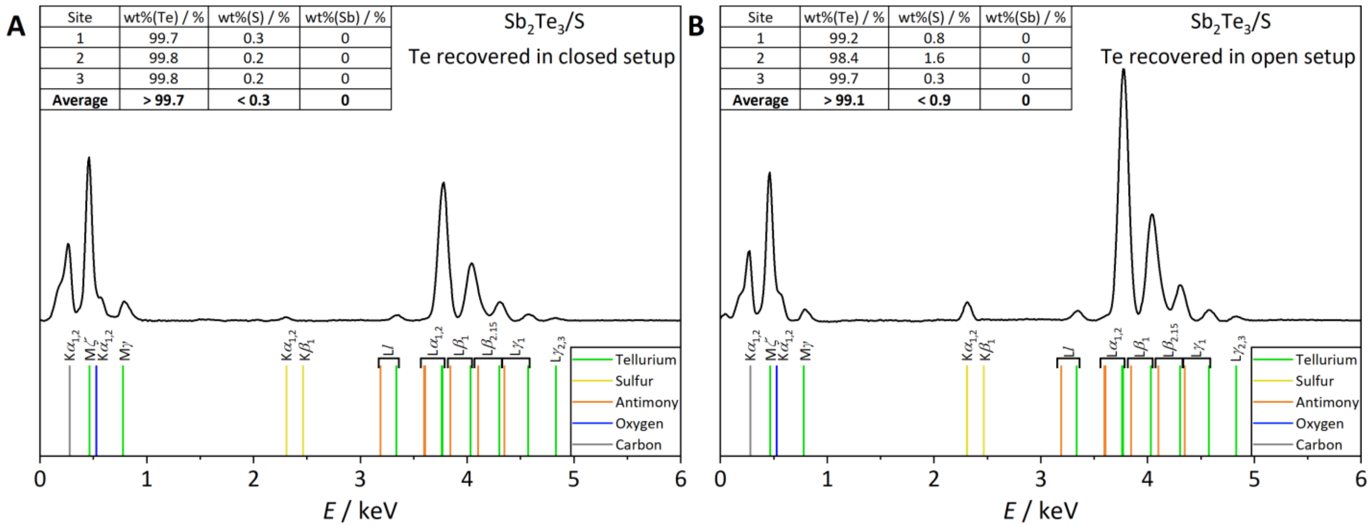


A

| Site | wt%(Te) / % | wt%(S) / % | wt%(Sb) / % |
|---|---|---|---|
| 1 | 99.7 | 0.3 | 0 |
| 2 | 99.8 | 0.2 | 0 |
| 3 | 99.8 | 0.2 | 0 |
| **Average** | **> 99.7** | **< 0.3** | **0** |

B

| Site | wt%(Te) / % | wt%(S) / % | wt%(Sb) / % |
|---|---|---|---|
| 1 | 99.2 | 0.8 | 0 |
| 2 | 98.4 | 1.6 | 0 |
| 3 | 99.7 | 0.3 | 0 |
| **Average** | **> 99.1** | **< 0.9** | **0** |

Figure S22: EDX-data of tellurium recovered in (A) the best-performing closed $Sb_2Te_3$/S experimental setup and (B) the best-performing open $Sb_2Te_3$/S experimental setup. For each sample, an average wt% value is given. It is calculated from three different measuring spots. X-ray emission lines are also shown for tellurium, sulfur, antimony, oxygen, and carbon as references.[5]

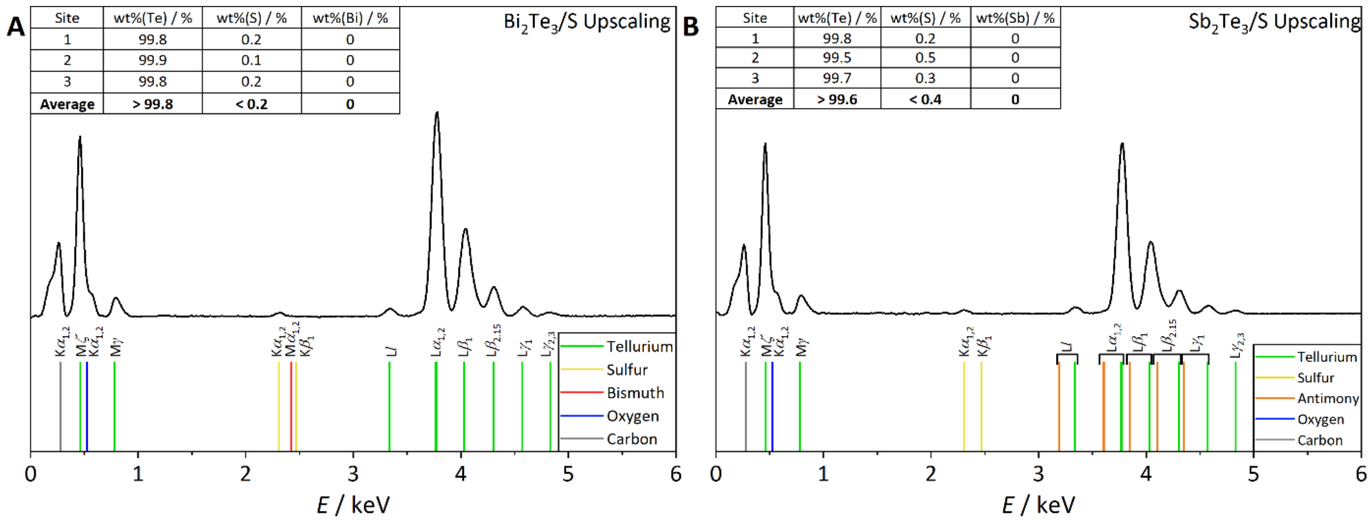


A

| Site | wt%(Te) / % | wt%(S) / % | wt%(Bi) / % |
|---|---|---|---|
| 1 | 99.8 | 0.2 | 0 |
| 2 | 99.9 | 0.1 | 0 |
| 3 | 99.8 | 0.2 | 0 |
| **Average** | **> 99.8** | **< 0.2** | **0** |

B

| Site | wt%(Te) / % | wt%(S) / % | wt%(Sb) / % |
|---|---|---|---|
| 1 | 99.8 | 0.2 | 0 |
| 2 | 99.5 | 0.5 | 0 |
| 3 | 99.7 | 0.3 | 0 |
| **Average** | **> 99.6** | **< 0.4** | **0** |

Figure S23: EDX-data of tellurium recovered in (A) the open $Bi_2Te_3$/S upscaling setup and (B) the open $Sb_2Te_3$/S upscaling setup. For each sample, an average wt% value is given. It is calculated from three different measuring spots. X-ray emission lines are also shown for tellurium, sulfur, bismuth, antimony, oxygen, and carbon as references.[5]

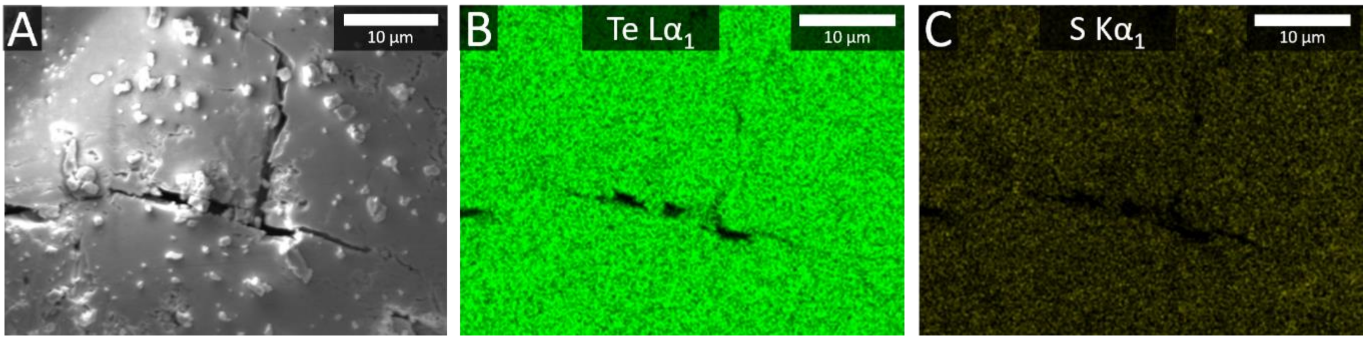


Figure S24: Elemental Mapping of a tellurium sample recovered in the best-performing open $Bi_2Te_3$/S experimental setup. Image (A) shows the electron image, image (B) shows the elemental mapping of the tellurium $L\alpha_1$ X-ray emission line and image (C) shows the elemental mapping of the sulfur $K\alpha_1$ X-ray emission line.

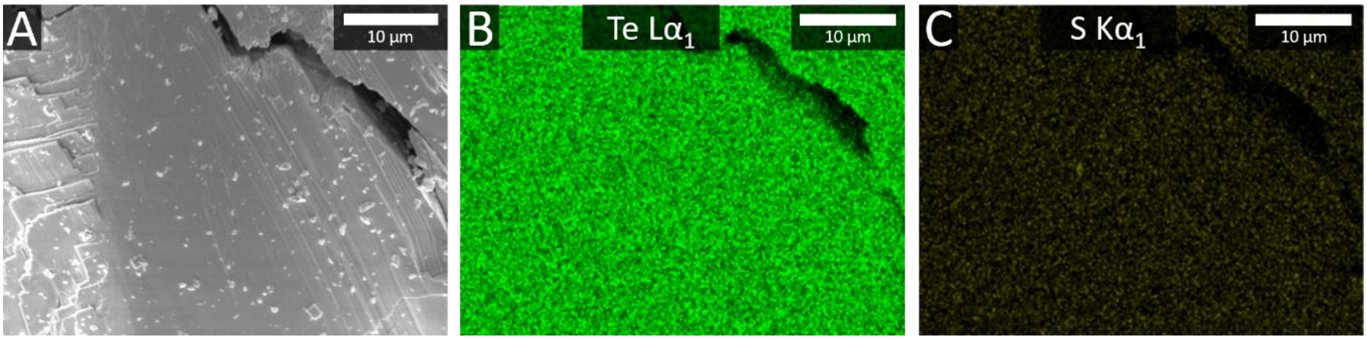


Figure S25: Elemental Mapping of a tellurium sample recovered in the best-performing closed $Sb_2Te_3$/S experimental setup. Image (A) shows the electron image, image (B) shows the elemental mapping of the tellurium $L\alpha_1$ X-ray emission line and image (C) shows the elemental mapping of the sulfur $K\alpha_1$ X-ray emission line.

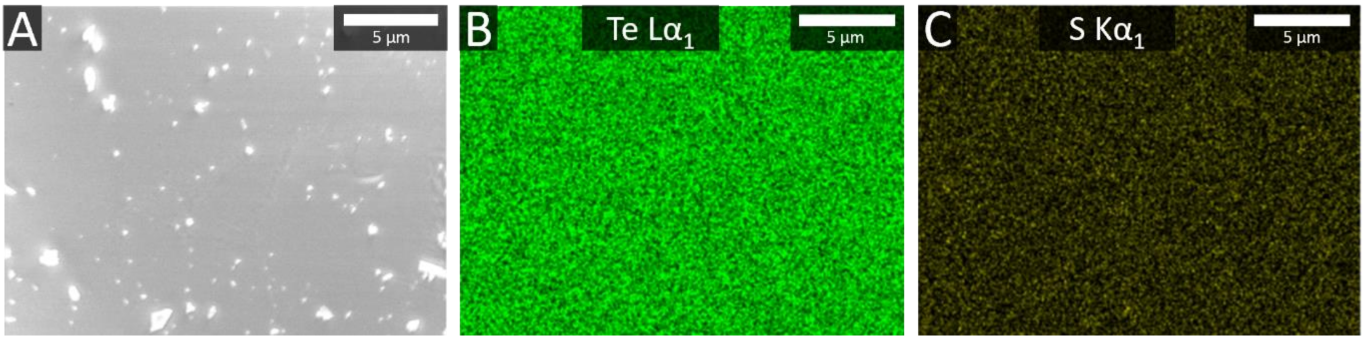


Figure S26: Elemental Mapping of a tellurium sample recovered in the best-performing open $Sb_2Te_3$/S experimental setup. Image (A) shows the electron image, image (B) shows the elemental mapping of the tellurium $L\alpha_1$ X-ray emission line and image (C) shows the elemental mapping of the sulfur $K\alpha_1$ X-ray emission line.

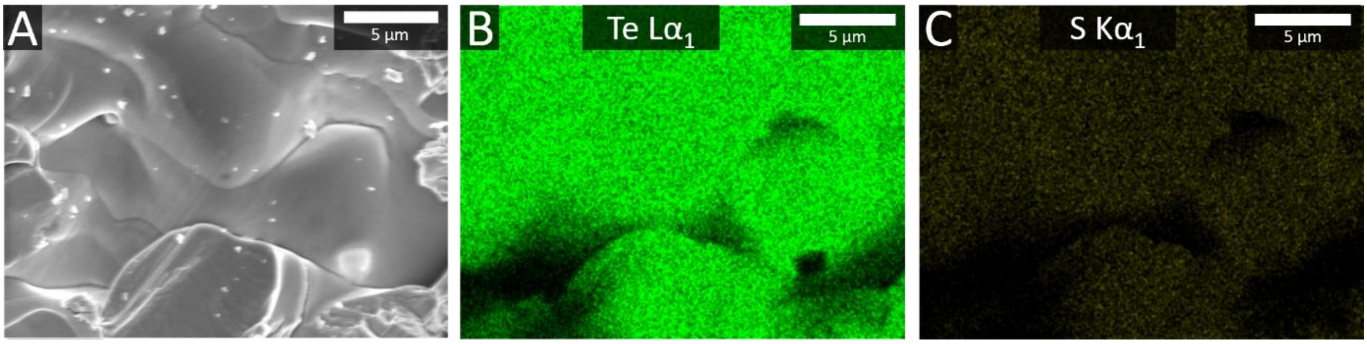


Figure S27: Elemental Mapping of a tellurium sample recovered in the open $Bi_2Te_3$/S upscaling setup. Image (A) shows the electron image, image (B) shows the elemental mapping of the tellurium $L\alpha_1$ X-ray emission line and image (C) shows the elemental mapping of the sulfur $K\alpha_1$ X-ray emission line.

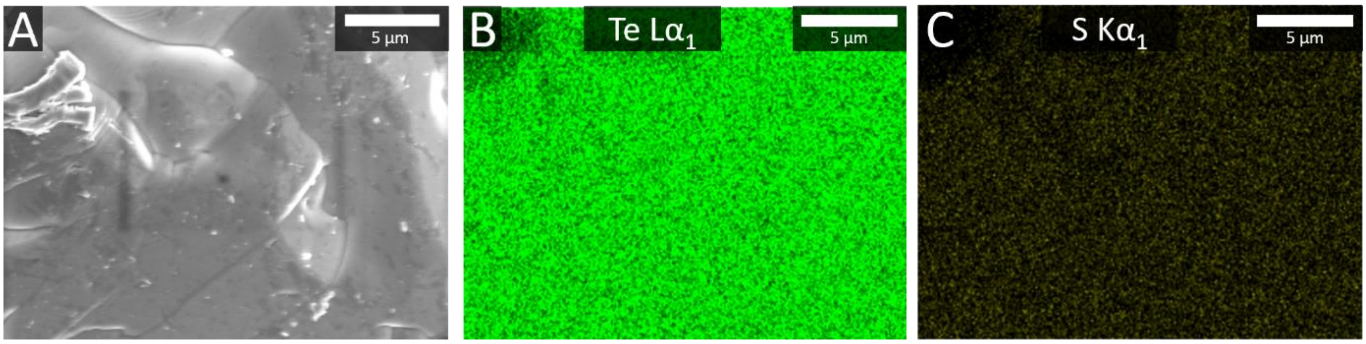


Figure S28: Elemental Mapping of a tellurium sample recovered in the open $Sb_2Te_3$/S upscaling setup. Image (A) shows the electron image, image (B) shows the elemental mapping of the tellurium $L\alpha_1$ X-ray emission line and image (C) shows the elemental mapping of the sulfur $K\alpha_1$ X-ray emission line.

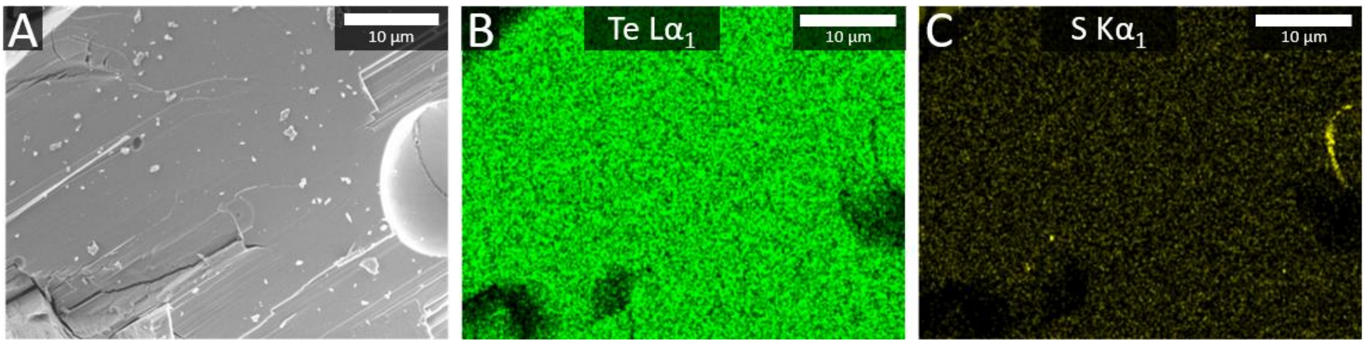


Figure S29: Elemental Mapping of a tellurium sample after a purification step at 425 °C. Image (A) shows the electron image, image (B) shows the elemental mapping of the tellurium $L\alpha_1$ X-ray emission line and image (C) shows the elemental mapping of the sulfur Kα1 X-ray emission line.

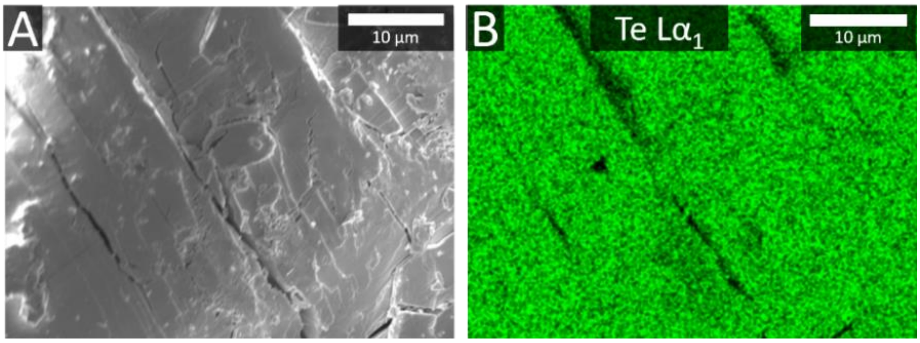


Figure S30: Elemental Mapping of a tellurium sample after a purification step at 500 °C. Image (A) shows the electron image, and image (B) shows the elemental mapping of the tellurium L$\alpha_1$ X-ray emission line.

## References

1 C. Adenis, V. Langer and O. Lindqvist, Acta Crystallograhica Section C, 1989, **45**, 941–942.
2 A. Kyono and M. Kimata, American Mineralogist, 2004, **89**, 932–940.
3 W. Hofmann, Zeitschrift für Kristallographie - Crystalline materials, 1933, **86**, 225–245.
4 B. E. Warren and J. T. Burwell, The Journal of Chemical Physics, 1935, **3**, 6–8.
5 J. A. Bearden, Rev. Mod. Phys., 1967, **39**, 78–124.